Soft Matter

Complex-type N-glycans on VSV-G pseudotyped HIV exhibit 'tough' sialic and 'brittle' mannose self-adhesions.

Journal:	*Soft Matter*
Manuscript ID	SM-ART-03-2019-000579.R1
Article Type:	Paper
Date Submitted by the Author:	18-Apr-2019
Complete List of Authors:	Abeyratne-Perera, Hashanthi; Howard University College of Medicine, Biochemistry and Molecular Biology Ogharandukun, Eric; Howard University, Chemical Engineering Chandran, Preethi; Howard University, Chemical Engineering

Complex-type N-glycans on VSV-G pseudotyped HIV exhibit 'tough' sialic and 'brittle' mannose self-adhesions.

Running title: complex-type N glycans have tough and brittle sugar self-adhesions

Hashanthi K. Abeyratne-Perera[1], Eric Ogharandukun[2], Preethi L. Chandran PhD [2,1]

[1] Biochemistry and Molecular Biology Department, College of Medicine

[2] Chemical Engineering Department, College of Engineering and Architecture

Howard University, Washington DC.

Corresponding author

Preethi L. Chandran, PhD
Assistant Professor
Department of Chemical Engineering, College of Engineering and Architecture, Howard University
Department of Biochemistry and Molecular Biology, College of Medicine, Howard University

Address:
1011 LK Downing Hall
2300 6th Street, NW, Howard University
Washington, DC 20059.
Email: preethi.chandran@howard.edu
Phone: 202-806-4595

ABSTRACT

The complex-type glycan shields of eukaryotic cells have a core layer of mannose residues buried under tiers of sugars that end with sialic acid (SA) residues. We investigate if the self-latching of mannose residues, earlier reported in pure monolayer studies, also manifests in the setting of a complex-type glycan shield. Would distal SA residues impede access to the mannose core? The interactions of mannobiose-, SA-, and lactose- coated probes with the complex-type VSV-G glycan shield on an HIV pseudovirus were studied with force-spectroscopy and gold-nanoparticle solutions. In force spectroscopy, the sugar probes can be forced to sample the depths of the glycan shield; whereas with sugar-coated nanoparticles, only interactions permitted by freely-diffusive contact occur. Deep-indentation mechanics was performed to verify the inferred structure of the engineered virus and to isolate the glycan shield layer for subsequent interaction studies. The adhesion between the sugar-probes and complex–type glycan shield was deconvoluted by comparing against the cross- and self-adhesions between the sugars in pure monolayers. Results from complementing systems were consistent with mannobiose-coated probes latching to the mannose core in the glycan shield, unhindered by the SA and distal sugars, with a short-range 'brittle' release of adhesion resulting in tightly-coated viruses. SA-coated probes, however, adhere to the terminal SA layer of a glycan shield with long-range and mechanically 'tough' adhesions resulting in large-scale virus aggregation. Lactose-coated probes exhibit ill-defined adherence to sialic residues. The selection and positioning of sugars within a glycan shield can influence how carbohydrate surfaces of different composition adhere.

INTRODUCTION

The surface of eukaryotic cells and viruses is covered with a layer of carbohydrates commonly referred to as the glycocalyx in host cells and glycan shield in pathogens. [1-3] The carbohydrate layer is comprised of strings of oligosaccharides or glycans which are attached to trans-membrane proteins via the N-glycosylation pathway [4, 5]. The N-glycosylation pathway occurs in two stages. During the first stage, a preformed oligosaccharide complex is transferred to an asparagine residue in a conserved motif of the nascent protein [6, 7]. The preformed complex has a core of three mannose residues [8]. During the second stage of the pathway, the sugar residues distal to the mannose core are trimmed off and non-mannose sugars are serially added in two branches. The N-glycosylation pathway produces three types of N-glycans: a high-mannose type where both branches are rich in mannose; a complex-type where both branches have galactose and glucosamine residues, and are commonly capped with sialic acid (SA) (see example in Fig. 1A); or a hybrid type where both high-mannose and complex branches are present [9, 10]. The N-glycosylation pathway has two implications for the sugar positioning within a glycan shield: one, the carbohydrate cover would ubiquitously retain a core layer of mannose residues; and two, the surface residues could be either mannose or SA. We had recently reported that opposing monolayers of mannobiose (disaccharides of mannose) residues exhibit strong self-latching adhesion [11]. We seek to find if similar self-latching manifests in the context of a complex-type carbohydrate cover where the mannose layer can be buried under layers of non-mannose sugars. Does the terminal sialic acid on a complex glycan shield abet or hinder access to the mannose core? Do the two predominant capping sugars, mannose and SA, cross-interact with each other? Does the type of N-glycosylation predetermine how the carbohydrate layers interact, independent of receptor-mediated interactions? The pioneering observations on carbohydrate self-adhesion mostly focused on charged sugars like the acidic glycans of proteoglycans and glycosphingolipids expressed on cell surfaces[12-21]. However, there are few studies on the self-adhesion between uncharged sugars like mannose and on the surfaces of viruses, where research has mostly focused on carbohydrate-lectin interactions.[22 23]

In this study, we investigate from a biophysical standpoint how a complex-type glycan shield interacts with sugar-coated probes, as a step during delineating the sugar-sugar interactions between two carbohydrate covers. By testing interactions with different sugar-coated probes, instead of another glycan shield, we can seek out principles of glycan-shield architecture and interactions that are general and can be extrapolated to a wider class of carbohydrate covers.

The specific complex-type glycan shield being probed is that of a replication-deficient HIV-1 virus pseudotyped with VSV-G proteins. The inferred organization of the pseudovirus and glycan shield is described below.

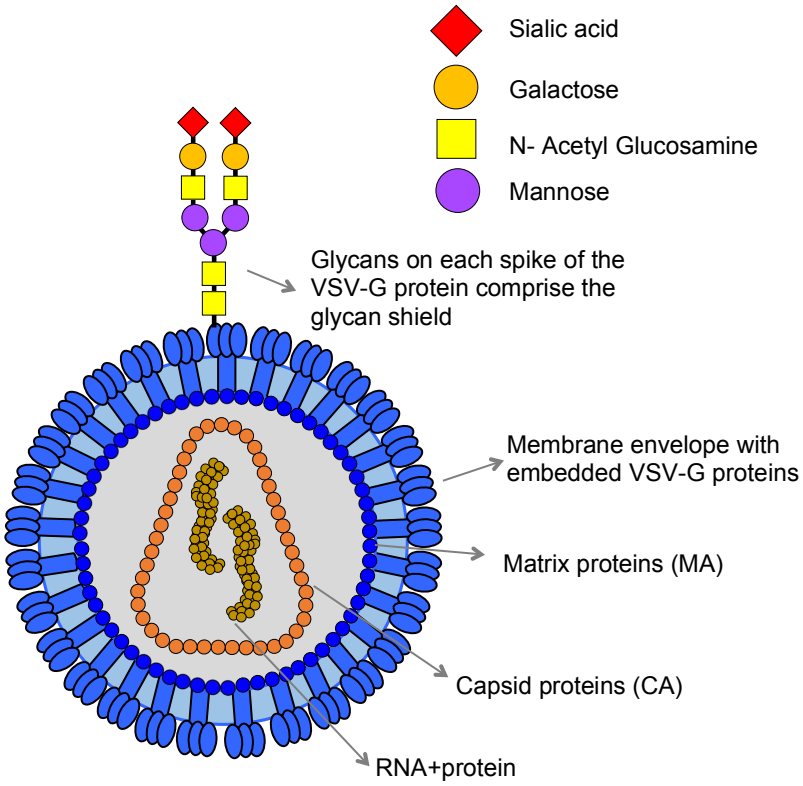

Figure 1:Purported structures of HIV-1 R- E- / VSV-G.
The HIV-1 R^- E^- / VSV-G pseudovirus is expected to have the structure of a wild-type HIV-1 virus, but the glycan shield of VSV-G. The structure of the HIV-1 virus consists of a membranous envelope lined with a thin lattice of matrix proteins (MA) on the inner surface [24]. Inside the membrane-envelope is a conical capsid or shell made up of capsid proteins (CA). The capsid houses the genomic RNA and associated protein. The glycan shield of the pseudovirus is comprised of glycans protruding from VSV-G proteins embedded in the membrane. The VSV-G protein is a trimer, with a complex-type glycan on each monomeric spike. The series of sugars in the complex-type glycan include a core of mannose residues and surface sialic acid (SA) residues [25].

The HIV-1 pseudovirus genome was rendered replication-deficient via deletions and mutations in its *nef* (negative regulatory factor) and *vpr* (viral protein R) genes that are essential for viral replication and pathogenesis, respectively [26-29]. The display of gp120 proteins was completely eliminated by a frameshift mutation in the *env* gene [30]. Instead, the virus was pseudotyped (i.e.

engineered to display envelope proteins from a foreign virus) with the membrane glycoproteins or 'G' proteins from the vesicular stomatitis virus (VSV) [26]. Pseudotyping with VSV-G proteins expands the host-selectivity of the HIV pseudovirus as VSV-G proteins bind LDL (low-density lipoprotein) receptors found on a wider range of host cells and cell-lines, including the HEK 239T cells in which the virus was grown [31-33]. Since these modifications do not affect the structural genes in the virus genome, the HIV-1 R^- E^- / VSV-G pseudovirus is inferred to be structurally organized like the wild-type HIV-1 virus, but with a glycan shield composed of VSV-G glycans (Fig. 1).

The pseudovirus in this study is expected to have the same structure as a wild-type HIV-1 virus, which consists of a membranous envelope enclosing cone-shaped shells or capsids. The membrane envelop is lined with a thin lattice of matrix proteins (MA) on the inner surface [34]. The capsids house the protein-bound genomic RNA of the virus [35, 36] (Fig. 1). The makeup of the pseudovirus glycan shield can be inferred from what is known about the VSV-G protein. The VSV-G protein is a classic example of a complex-type glycoprotein where the mannose core is capped by a sequence of N-acetyl glucosamine, galactose, and terminal sialic acid residues (Fig.1) [10, 37, 38]. Studies have reported that the composition of the VSV-G oligosaccharide chains is relatively unaffected by the type of host cell in which the virus was synthesized [37]. The G protein is a trimer, with each protruding spike of the monomer containing two copies of the complex-type glycans; the glycans alone constitute ~10% of the glycoprotein by weight [37, 39].

Our study is organized into two parts. In the first part, as a prelude to the glycan-interaction studies, we characterize the pseudovirus response to indentation for the specific genomic modification, pseudotyping, and testing conditions. The characterization is necessary for two reasons. First, the specific pseudovirus has not been morphologically or structurally studied before, and we need to verify if it is organized similarly to a wild-type HIV-1 virus. Secondly, we need to identify how best to sample the glycan shield layer alone for subsequent sugar-interaction studies. From a material-mechanics standpoint, the HIV-1 virus is a soft fluid-filled shell enclosing another shell (capsid). It is not clear if an indenting probe would compress the virus as a whole, penetrate through individual layers, or simply squeeze the internal fluid out. By understanding how the virus organization responds to probe-indentation, we can set controls so that the depths of the glycan shield alone is effectively sampled for the interaction studies in the second part.

In the second part of the study we investigate the interactions of the glycan shield with probes coated with one of three sugars (Figure 2): (i) SA which is present on the outer surface of the pseudovirus glycan shield, (ii) mannose disaccharides or mannobiose which are present at the core of the glycan shield, and (iii) lactose, a disaccharide of glucose and galactose, which is included as a control for mannose- and SA- specific interaction patterns. Galactose is also present in the glycan shield. We will study the interactions in both the enforced environment of atomic force spectroscopy, where the sugar probe is forced to contact all sugar tiers within the virus glycan shield, and in unenforced environment where sugar-coated probes are free to diffuse and interact with the glycan tiers they have access to. The cross- and self- interactions between pure sugar monolayers will provide context for interpreting how the sugar-probes traverse into the layers of the glycan shield.

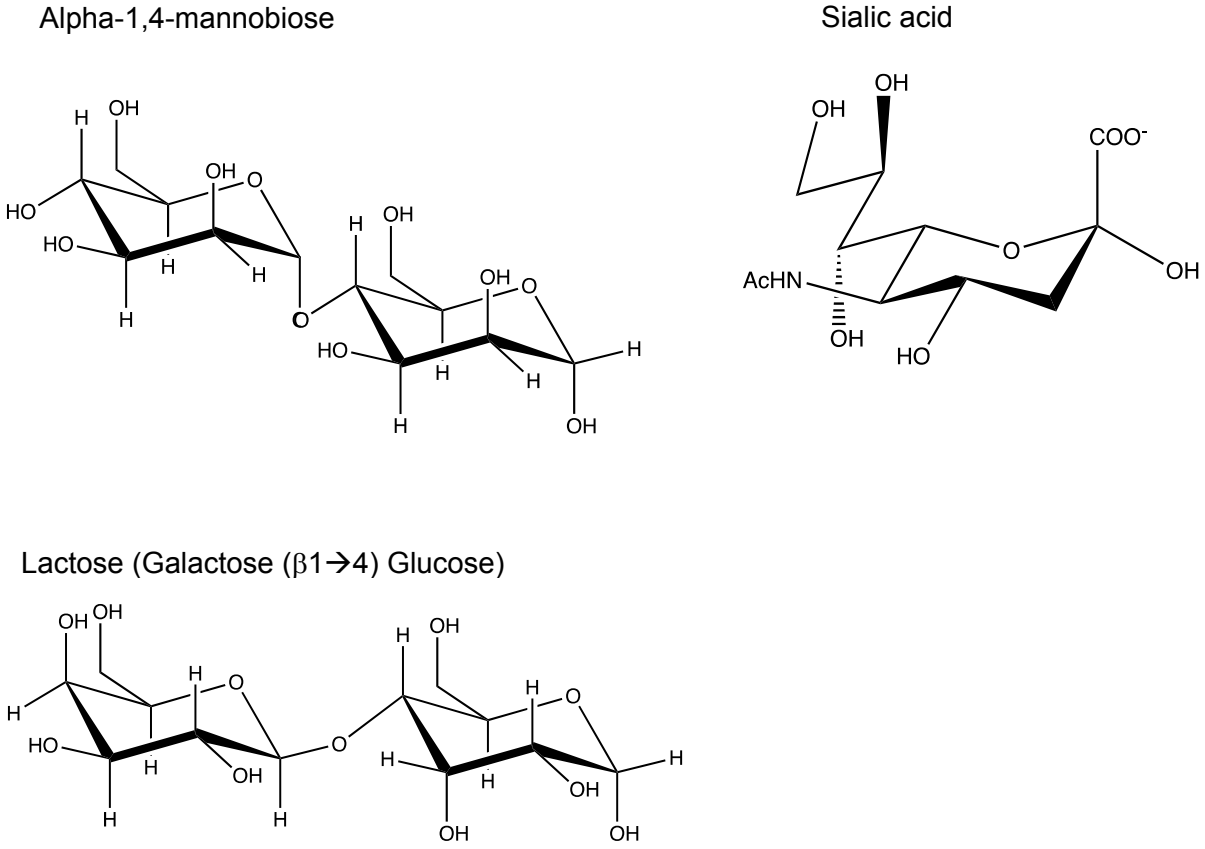

Figure 2: The chemical structures of three sugars (mannobiose, sialic acid and lactose) of which interactions with the glycan shield are tested in this study.

MATERIALS AND METHODS

Generating replication-deficient HIV-1 Luc R- E- / VSV-G or pseudo virus particles

Pseudovirus was generated in Dr. Sergei Nekhai lab at Howard University as described in the Charles et al. [26] by co-transfecting the HEK293T cells with two expression vectors: (i) pNL4-3. $Luc^{-}.R^{-}$ E^{-} generated by inserting firefly luciferase gene into the *nef* gene of the HIV-1 genome and two frame shift mutations to render the clone env^{-} and vpr^{-}; and (ii) pHEF VSV-G which expresses the envelope glycoproteins from VSV. The released virus particles were collected from the supernatant after 72 hours.

Covalent attachment of sugars on gold coated AFM probes and AFM surfaces

4-azido-2,3,5,6-tetrafluoro-N-(2-mercaptoethyl) benzamide or ATFMB linkers were synthesized as described in Aberyatne-Perera et al., 2017 (10). Briefly, gold-coated AFM probes (NPG-10, Bruker Inc., Billerica, MA) and AFM surfaces were thoroughly rinsed with 95% ethanol and incubated for 12-15 hours in a saturated solution of freshly synthesized ATFMB dissolved in ethanol in order to form self-assembled-monolayers. The probes were then rinsed with ethanol and transferred to a clean petri-dish with 200 μl of 20 mg/ml of either alpha -1,4- mannobiose (Dextra Inc., Reading, U.K.), lactose, or sialic acid (Millipore Sigma Inc., St. Louis, MA) solutions. The surfa ces were irradiated with UV (254nm wavelength) from an 8 Watt UV lamp (Thermofisher Scientific Inc., Waltham, WA) for 10 minutes. The distance between the UV lamp and the probe was maintained approximately at 3 cm. When UV irradiated, sugar residues in solution crosslink to the aryl-azide groups at the free ends of the self-assembled linkers on the probe surface. The functionalized AFM probes were then rinsed with MilliQ water to remove unattached sugars.

Nano-indentation and Force Spectroscopy

6 μl of the undiluted pseudovirus solution was allowed to adsorb on aminopropylsilane-functionalized mica, by incubating for about 10 minutes, followed by washing with 1 ml of pure water to wash off the excess/unabsorbed virus particles [40].The virus-adsorbed surfaces were then overlaid with about 100 μl of water or 150 mM NaCl and immediately mounted on the AFM stage for testing within 1 hour. Samples were changed every hour. Nano-indentation and force spectroscopy experiments were performed with a Multimode/ PicoForce system (NS-V controller, Bruker Nano-surfaces Inc., Santa Barbara, CA) in a fluid cell filled with either water or 150 mM NaCl. The deflection sensitivity of gold-coated NPG-10 cantilevers (Bruker Inc.,

Billerica, MA) was determined by indenting on mica surface. Their spring constant (k) was obtained by standard thermal-tuning method. For deep nano-indentation probing of the virus structure, the ramp velocity was set to 50 nm/s and at least 25 nm cantilever deflection was achieved prior to retraction. Only the deep-indentation studies done in 0 mM NaCl environment are presented in the paper, except for the case of deep-indentation with SA probes where the 150 mM NaCl data is presented. For force spectroscopy probing of the glycan-shield interactions, the indentation velocity was kept at 100 nm/s, and the cantilever deflection was specified to be no greater than 8 nm to avoid penetrating the virus membrane. In addition, the probe was allowed to linger at the sample surface with a 1 sec delay before retraction to give time for establishing interactions. The AFM force curves were analyzed with an in-house Matlab code described earlier [11]. At least 200 force curves were collected for both probe-virus and probe-monolayer experiments, from atleast three different sample preparations on mica, and with atleast two sampling areas per mica. The sampling points were spaced 30 nm apart so as to collect multiple force curves from the same virus as well as multiple viruses (virus diameter ~100 nm). Histograms of the data are presented.

Synthesis of sugar-stabilized gold nanoparticles

Three pre-labeled conical flasks containing 20 ml of ultrapure water (Genesee Inc., El Cajon, CA) were brought to a boil on a hot plate and 500 µl of 0.02 M $HAuCl_4$ (MilliporeSigma Inc., St.Louis, MA) was added to each with stirring. 18.5 mg of sialic acid, 20.5 mg of lactose, and 20.5 mg of mannobiose were separately dissolved in 500µl water in Eppendorf tubes, and 50 µl of 1 M NaOH was added to each. Each sugar solution was added to a pre-labeled flask of boiling $HAuCl_4$ solution with vigorous stirring. The solution develops a reddish color as sugar-coated nanoparticles form. When the colors are fully developed, the flasks were removed from the hot plate and allowed to cool. The solutions were centrifuged at 8000 RPM for 15 minutes to isolate the nanoparticles, which were then re-suspended in ultrapure water and stored at 4^0 C.

UV-Vis spectroscopy

3ml of the sugar-stabilized nanoparticles were transferred to a glass cuvette and the surface plasmon resonance (SPR) was measured with a Cary 60 UV-VIS spectrophotometer (Agilent Inc., Santa Clara, CA) against a water blank. The measurements were repeated after mixing the nanoparticles with 10 µl of 1:100 dil. of $1x10^7$ / ml viral titers.

Dynamic light scattering (DLS)

DLS measurements of nanoparticle solutions (1 ml), and of nanoparticle + virus solutions (10µl of 1:100 dil of $1x10^9$ viral titer + 1 ml of nanoparticle solution) loaded in quartz cuvettes (Malvern Instruments, Inc., Westborough, MA) were performed with a Zetasizer ZSP (Malvern Instruments, Inc., Westborough, MA) at 633 nm wavelength and 173° back-scatter angle. Plain virus solutions were loaded in 40µl disposable cuvettes (Malvern Instruments, Inc., Westborough, MA) for DLS measurements. All samples were first brought to room temperature and then equilibrated at 25° C for 5 minutes in the instrument before measurements. The duration of data collection was 1500 sec. The instrument laser attenuation, sampling position, and sampling time were maintained constant for all measurements. DLS measurements produce an intensity correlation curve, which has an exponential fall for every discernible diffusion size in the solution. The exponential drop shifts towards larger time intervals (i.e., moves right) as the speed of the diffusing species decreases. The DLS correlation curves were analyzed with an in-house Matlab-based software to extract the hydrodynamic diameters of the different diffusing populations present in a sample. The hydrodynamic diameter is the size of a Stokesian bead having the same diffusion speed as the species in solution [41].

RESULTS

1. Structural characterization of virus by deep nano-indentation with a bare AFM probe

While there are comprehensive studies characterizing the structure and mechanics of the native HIV virus,[42, 43] there has not been much organizational and mechanical characterization of the VSV-G pseudotyped HIV. Few studies have noted that the centrifugal resistance and stability of the virus changes with the pseudotyped envelop protein.[44, 45] We need to determine how the virus with the specific genomic mutation and preparation conditions responded to indentation, under the solution and testing conditions of our study, so that the glycan shield alone can be accessed for subsequent force spectroscopy studies. AFM dry imaging confirmed that the pseudovirus had a similar structural organization of the wild-type virus (core capsid within the membrane) and the overall morphological dimensions were in the range expected (Suppl. Info. 1).

A base-line deep-indentation study of the virus was performed with a bare AFM tip. A monolayer of virus particles was adsorbed on a mica surface maintained in a fluid environment. As shown in the schematic of Fig. 3A, a bare AFM probe is sharp compared to an adsorbed virus; the probe is about 2nm wide at the tip whereas the virus is about 100nm wide. Based on its inferred structure, we expect the following virus layers to be presented to the approaching probe: (i) the carbohydrate layer due to the glycans bound to VSV-G proteins, (ii) a lipid membrane bilayer that embedded with VSV-G proteins and lined with a lattice MA (matrix) proteins on the inside, and (iii) the HIV-1 capsid with the viral RNA genome inside [46]. Fig. 3B shows the force resisting the probe as it approaches into (blue curve) and retracts away (red curves) from the layers of organization of a representative virus. The x-axis shows the separation, which is the distance between the tip of the AFM probe and the surface of the mica on which the virus is adsorbed. If the AFM tip were compressing all layers of the virus as one whole, the approach force curve will increase monotonically with indentation. Instead, the approach force increases unevenly, suggesting that the tip is sequentially penetrating and sampling the interaction of each virus layer, with the approach force rising and falling as each layer initially resists and eventually gives in to penetration by the AFM tip (Fig.3C).

***Penetrable glycan shield and membrane*:** As the probe approaches the surface-adsorbed virus, it first encounters a force resistance at ~28 nm away from the surface (Fig. 3B). The resisting force increases gradually but at separations of ~15 nm, shows a sharp rise and fall, and settles into a plateau profile. Such break-through events (sharp rise and fall in forces) have been observed in membranous structures and occur as the probe cuts through the spikes of the glycoproteins and penetrates the membrane[47, 48]. The breakthrough-force followed by plateauing was observed to occur around 1.45 ± 0.2 nN (Fig. 3B n=10 viruses). At these values, membrane penetration force of the pseudovirus is an order higher than that of the influenza virus (~0.1nN) [47], but much lower than that of the HEK293T cells (10 – 30nN) [48]. Since the pseudovirus was grown in HEK293T cells, at an initial glance our data suggests that the viral membrane may be floppier than the host membrane from which it was derived. We note that the indentation rate was 300nm/s for HEK293T membranes and 50nm/s in our case. Following the membrane break-in, the force plateaus (i.e., the resistance remains the same as the tip moves down the virus) for anywhere between 3 to 7nm of indentation into the virus (examples of indentation curves from several viruses are shown in Fig. 4A). The plateauing of the indentation resistance can be attributed to a combination of penetration into a lipid membrane (resistance in fluid does not increase with indentation depth but with indentation rate, which is constant here) and buckling of the MA lattice (the shell wall deflects inwards at constant force). A well-developed plateau such as that shown in Fig. 3B has about a 6nm length, which is in the range of the combined thickness of the membrane (~4nm) and MA (~3nm) layers of the HIV-1 virus as inferred from electron density maps [49].

If the plateau force region is attributable to membrane penetration, one expects the next force contribution coming from deforming or penetrating the capsids. After penetrating the membrane, the indentation force increases but with at least two intermittent falls, suggesting a combination of compressing and penetrating of the capsid shell. The average height of this seemingly indented capsid layer is ~6nm, much smaller than the expected 40nm cross-sectional diameter of HIV capsids [49, 50]. The collapsed height of these surface-adsorbed capsids suggests that they are mechanically floppy structures, which is also in line with reports that the lattice arrangement of the HIV capsid (CA) [51-53] and the capsid protein (CA) itself [54] are malleable structures.

In accordance with the interpretation that the probe penetrates collapsed membrane and capsids during the approach phase, we see jumps in force occurring during the retraction phase that suggests the release of the penetration (Fig.4B). The separation distances at which the

jumps occur are consistent with the size of uncollapsed capsid and membrane shells (~51-/+ 5 nm and ~113 -/+ 21 nm, respectively, n= 10 viruses) (Fig. 3B). The 50nm peak adhesion release could be coming from the tip pulling out the collapsed capsid to its non-collapsed dimensions before letting go. The 100nm total adhesion length can be attributed to the net height of the collapses virus and/or to the release of membrane tethers.

The indentation analysis provides context for subsequent force-spectroscopy studies in two ways. First, it suggests that for our particular case of virus type, preparation, and testing conditions, the virus is collapsed on the surface; and at 50nm/sec indentation rate the probe penetrates layers of the virus organization instead of compressing the virus as a whole. Secondly, the region of glycan-shield penetration can be identified as occurring prior to the more distinctive region of membrane penetration marked by force jumps and plateaus. This glycan-shield region extends as far as ~10nm (see more virus force curves presented in Fig. 5); and the force is commensurate to the elastic modulus of about 10s of kPa, which is the range expected for soft hydrogels.[55, 56] The length and resistance of the glycan shield region suggest that the glycans are not collapsed on the virus surface but are rather protruding out as a ‘shield’. To further confirm the glycan presentation, the viruses were indented with different sugar-coated probes (see section below). We note that the mannose-binding lectin Con A did not bind and aggregate the pseudovirus (data not shown), which is consistent with SA, not mannose, being the distal residue in the glycan shield and with reports that SA residues masks Con A binding to mannose residues.[57]

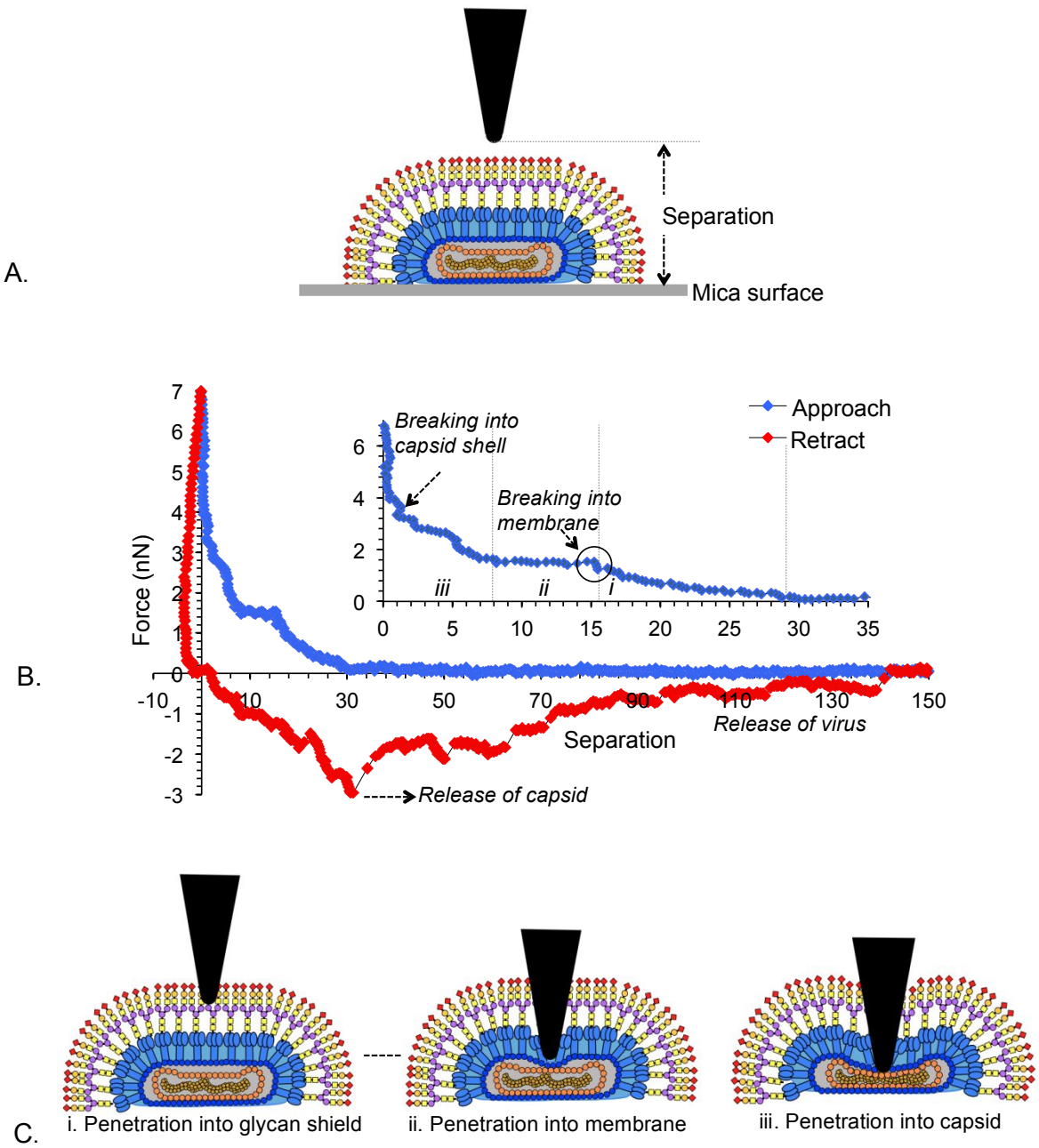

Figure 3: Nano-indentation of the virus with a bare AFM probe.
(A) Schematic showing the layers of viral organization presented to a sharp indenting probe. (B) Force curves showing the resistance to indentation and retraction of the probe at different separation distances. Three regions of force changes can be distinguished in the approach curve, related to the penetration into and buckling of the different shell layers. As the probe retracts, it releases the penetrated shells with large jumps in forces at separations corresponding to uncollapsed capsid and virus dimensions. (C) Schematic depicting the possible penetration and buckling of virus layers that occur during each force region in the approach curve.

Deep indentation with sugar-coated AFM probes affirms sampling of glycan shield*:* Figure 4A shows examples of the approach force curves seen during bare-tip indentation of different viruses. The three regions corresponding to glycan shield, membrane, and capsid mechanics can be distinguished from the non-monotonic force rises. While the depth of each region can change (for instance depending on where the virus is indented), the penetration into the membrane and subsequent plateauing occurs around 1.45 ± .2nN (n~10 viruses). In other words, the glycan shield layer can be sampled as the gel-like layer prior to penetrating the membrane at ~1.5nN. To further corroborate the sampling of the glycan shield, the virus was indented with sugar-coated probes. Deep indentation with sugar-coated probes produced force ranges that were largely similar to those from bare tips (Fig. 4B), though the membrane break-through and subsequent plateauing were not clearly visible with SA-coated tips (consistent with surface-interaction findings described later in Sec. 2A). Lactose-tips showed virus membrane break-in at 1.19 +/- 0.3 nN (n ~ 5 viruses). With mannobiose-coated tips, a plateauing of the force occurred at 1.15 +/- 0.07nN (n ~ 5 viruses) in the region of membrane breakthrough/buckling (black arrows in Figs. 4B and C), and an additional force drop appearing in the middle of the region attributable to the glycan shield (red arrows in Figs. 4B and C). This new force drop occurs at ~3nm before the membrane penetration occurs, and it's positioning is consistent with the expected location of the mannose core half way into the glycan shield. The force drop in the glycan shield region could reflect the penetration of the mannose core by the mannobiose-coated probe in ways similar to that observed between two pure mannobiose monolayers in similar low salt conditions [11]. At 0.53 +/- 0.1 nN, the penetration force that occurs in the glycan shield would be less than the ~1.1 nN break-in forces observed for self-penetrating pure mannobiose monolayers [11]. In addition to having non-mannose sugars, the mannose-mannose linkage in the glycan shield (α 1-3 and α 1-6) is different than that of the mannose-mannose linkage in the sugar probes (α 1- 4), which could be resulting in the lower break-in forces. The deep profiling of the virus with both bare- and sugar-coated probes suggests that the glycan shield can be sampled without penetrating into the membrane and at least up to the level of the mannose core, if the indentation force were restricted to 1nN. Establishing the upper indentation force is important for the sugar-interaction studies below. While it is critical to sample the depths of the glycan shield, it was equally critical to avoid penetrating the cell membrane underneath and misinterpret the release forces from membrane penetration to the release of adhesion forces with the glycan shield.

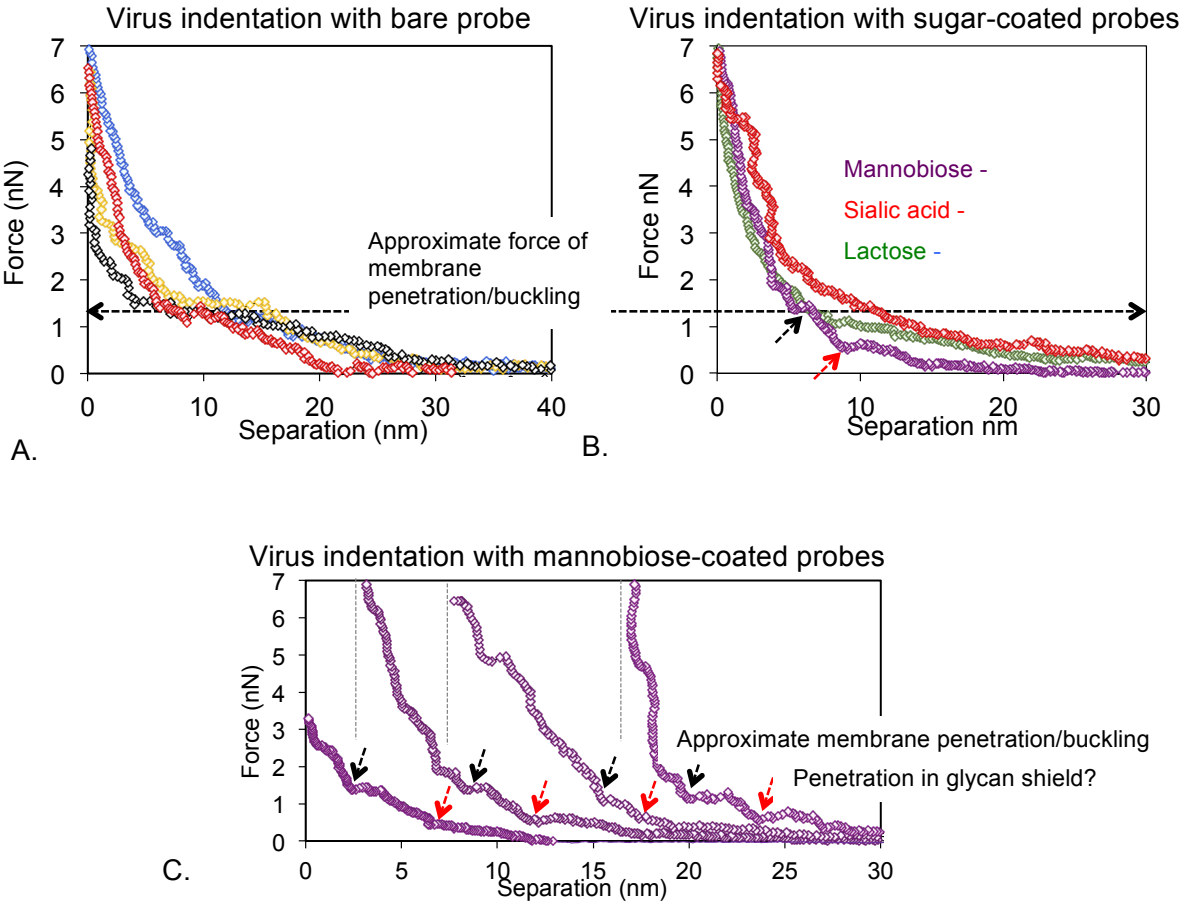

Figure 4: Deep nanoindentation of the virus with sugar-coated probes.
(A) Approach force curves from the bare-tip indentation of multiple viruses showing the occurrence of the membrane-penetration/buckling plateau at around 1.5nN. (B) Examples of the approach force curves obtained when the virus was indented with sugar-coated tips. The purple, green, and red curves correspond to indentation with mannobiose, sialic acid, and lactose-coated AFM tips respectively. Indentation with sialic-acid coated tips did not produce a well-defined force plateauing at 1.5nN. Indentation with mannobiose-coated tips however produced an additional force-drop within the region corresponding to the glycan shield. Black arrow points to force-drop due to membrane penetration/buckling and black arrow points to the new force drop occurring in the glycan shield. (C) Examples of several indentation approach curves taken with mannobiose-coated probes. A force drop at .65nN (red arrow) appears ~3nm before the membrane penetration/buckling plateau at ~1.5nN (black arrow).

2. Sugar-sugar interactions with a glycan shield

Our goal is to understand if the positioning of the sugars in a virus glycan shield affects its adherence with another glycan shield or glycocalyx, independent of receptor-mediated interactions. In the first part of this section, we performed force spectroscopy on the glycan shield alone to infer its interaction patterns with three sugar-coated probes from their respective

adhesion release pattern. We deconvolve the probe interaction with the multiple tiers of sugars comprising the glycan shield by comparing against its interactions with 'single-tiered' sugar monolayers (Fig. 5). All interaction studies are performed in both water (Fig. 6) and 150mM salt (Fig. 7). This is because salt has opposite effects on two fundamental mechanisms governing sugar-sugar interactions: hydrogen bonding and charge. Salt ions decrease the former (by interfering with dipole interactions) but increase the latter (by decreasing charge repulsion and increasing charge-bridging effects). By tracking the differential salt effect, the mapping between glycan-shield and pure monolayer studies can be verified. In force spectroscopy experiments, the sugar-coated probes can be forced to make contact with the depths of the glycan shield, and produce interaction patterns that might not be relevant in natural environments where the probe (or carbohydrate cover) diffuses freely and might not access the deeper sugars of the glycan shield. Therefore, in the second part of the study, we test if the affinity between virus and sugar-coated probes in freely-diffusive environments can be explained by the adhesion rules inferred from force-spectroscopy (Fig. 8).

2A. Interactions in enforced-contact conditions of force spectroscopy

Mannobiose residues do not significantly cross-interact with sialic acid monolayers:
Figure 5A shows a representative example of the force curves seen when a mannobiose-coated probe approaches and retracts from a monolayer of SA residues in 0mM and 150mM NaCl conditions. The setup mimics the mannobiose probe sampling the surface tier of SA residues in the virus glycan shield. In force spectroscopy, a negative spike in force occurs during the retraction phase should the two surfaces in contact resist separation. The integral of the negative forces over the separation distance is a measure of the adhesion energy or the work done to separate the two surfaces. There were very small negative forces during the retraction of mannobiose and SA surfaces in both salt and water medium, and the adhesion energies were on the order of a few kJ. Mannobiose and SA, two of the common distal sugars in glycan shield, do not appear to cross-interact. In contrast, the control lactose-probe showed significant retraction forces and adhesion energies with a SA-monolayer (Fig. 5B). These cross-interactions are discussed subsequently in the context of the lactose-probe and glycan shield interactions. Mannobiose did not have cross-adhesions with lactose residues in water (previously shown in ref.[11]) and in 150 mM NaCl (Suppl. Info. 3)

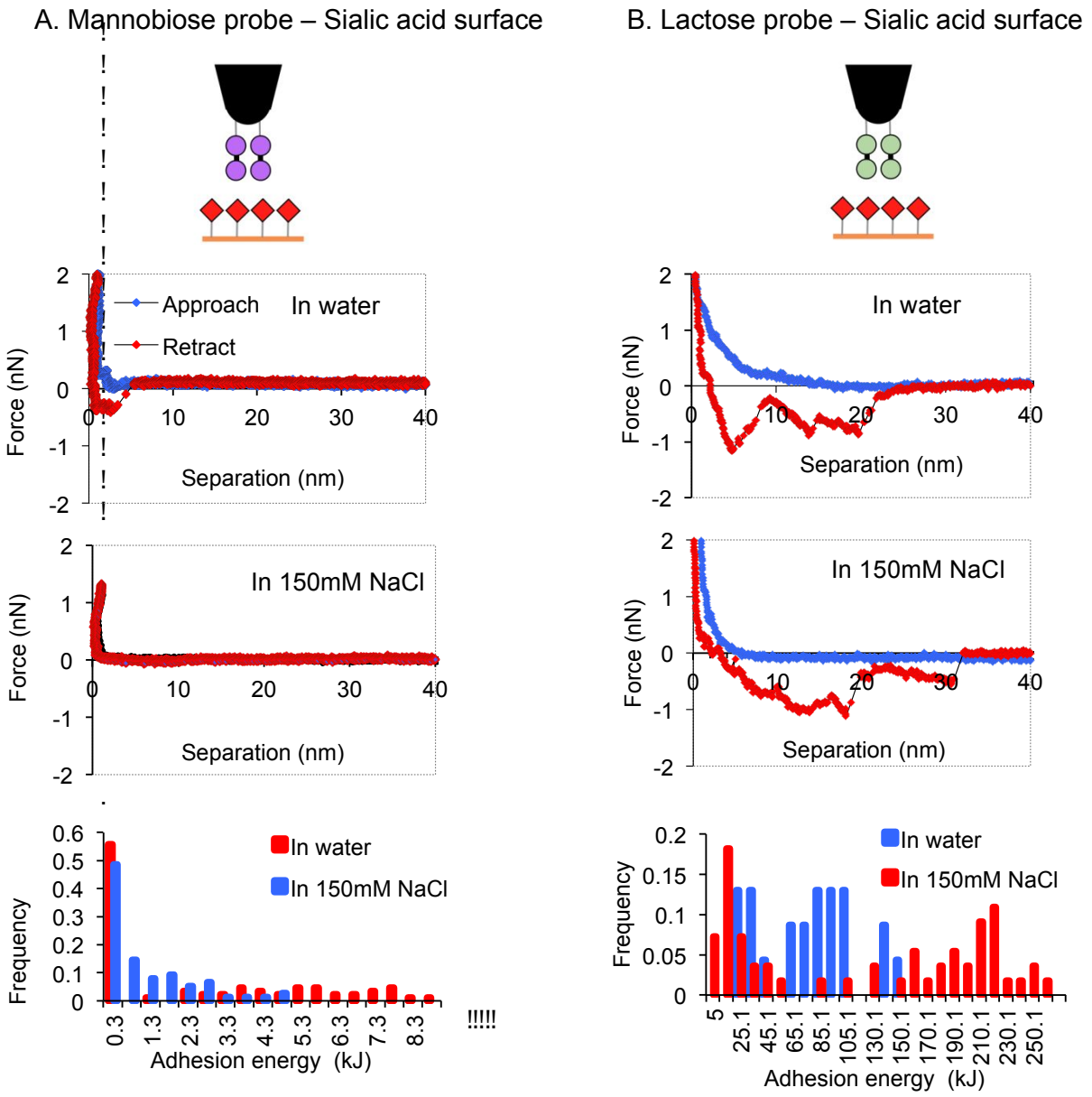

Figure 5: Cross interactions between sugar monolayers.
[A] The schematic (top), representative force spectroscopy curves in water and 150mM (middle), and histogram of average adhesion energies shown for when a mannobiose-coated probe approaches and retracts from a SA monolayer. There were no significant levels of negative forces observed during retraction and the distribution of adhesion energies were one the order of a few kJ, suggesting that there was no significant cross-interaction between sialic and mannobiose residues. [B] The schematic (top), representative force curves in water and 150mM (middle), and histogram of average adhesion energies shown for when a lactose-coated probe approaches and retracts from a SA monolayer. Large negative forces occur during retraction, and adhesion energies are distributed in the 10s and 100s of kJ for water and 150mM NaCl, respectively, indicating significant level of cross interactions occurring between lactose and SA sugar residues (n > 100 force curves).

Interactions between mannobiose-probe and virus glycan shield resemble self-interactions between two mannobiose monolayers: Consider a mannobiose-coated probe approaching a complex-type glycan shield (pictorial depiction in top panel of Fig. 6A). With insignificant cross-adhesion occurring with the tiers of sialic acid and galactose (inferred from the lack of interaction with lactose), one would suppose the probe to reach and interact with the mannose core, and upon retraction to produce the adherence characteristics representative of pure mannobiose-mannobiose monolayers. Abeyratne-Perera et al.[11] reported that the two mannobiose layers penetrated upon application of force and had two distinctive features: (i) the adhesion always released sharply with a peak break-out force close to the physical separation of the two layers, and (ii) salt supplementation decreased the occurrence of peak adhesion forces but not its base maximum (see self-monolayer interaction curves of Figs. 6A and 7A, and histograms in Suppl. Info. 1). When a mannobiose probe approaches and retracts from a glycan shield, we observed a single, large and immediate release of adhesion via a peak negative force, at both 0 and 150mM NaCl (Figs. 6A and 7A, bottom). The occurrence of the peak force decreases with salt supplementation (i.e., higher incidence of zero peak force, compare interaction histograms in Fig. 8). The similarities between how the mannobiose-probe retracts from mannobiose monolayer and from the glycan shield, the distinct pattern of mannobiose-mannobiose pullouts, along with the perceived lack of cross-interactions with SA and lactose layers, suggest that a mannobiose probe could be sampling the mannose core unhindered by distal sugars. This inference is also consistent with the earlier observation of a second break-through or latching event occurring within the region of glycan-shield penetration when the virus was indented deep with mannobiose-probes (Fig. 4C).

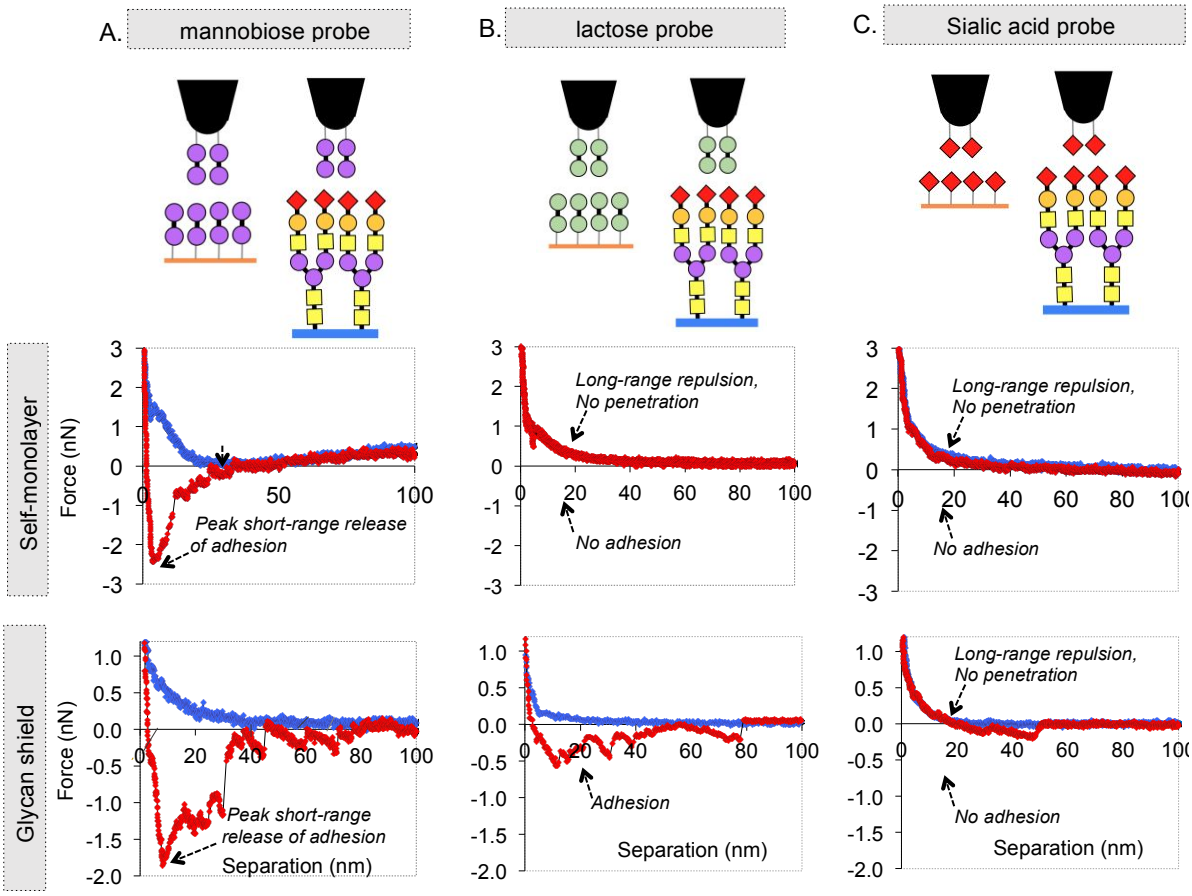

Figure 6: Interactions of a sugar-coated probe with the virus glycan shield and self-sugar monolayers in 0mM NaCl conditions. Approach force curves are shown in blue and retraction curves are shown in red. (A) Depiction of a mannobiose-coated probe approaching a mannobiose-coated surface and a virus glycan shield (top); and force curves resulting from probe interaction with the mannobiose monolayer (middle) and glycan shield (bottom). (B) Depiction of a SA-coated probe approaching a SA-coated surface and a virus glycan shield (top); and force curves resulting from probe interaction with the SA monolayer (middle) and glycan shield (bottom). (C) Depiction of a lactose-coated probe approaching a lactose-coated surface and a virus glycan shield (top); and force curves resulting from probe interaction with the lactose monolayer (middle) and glycan shield (bottom).

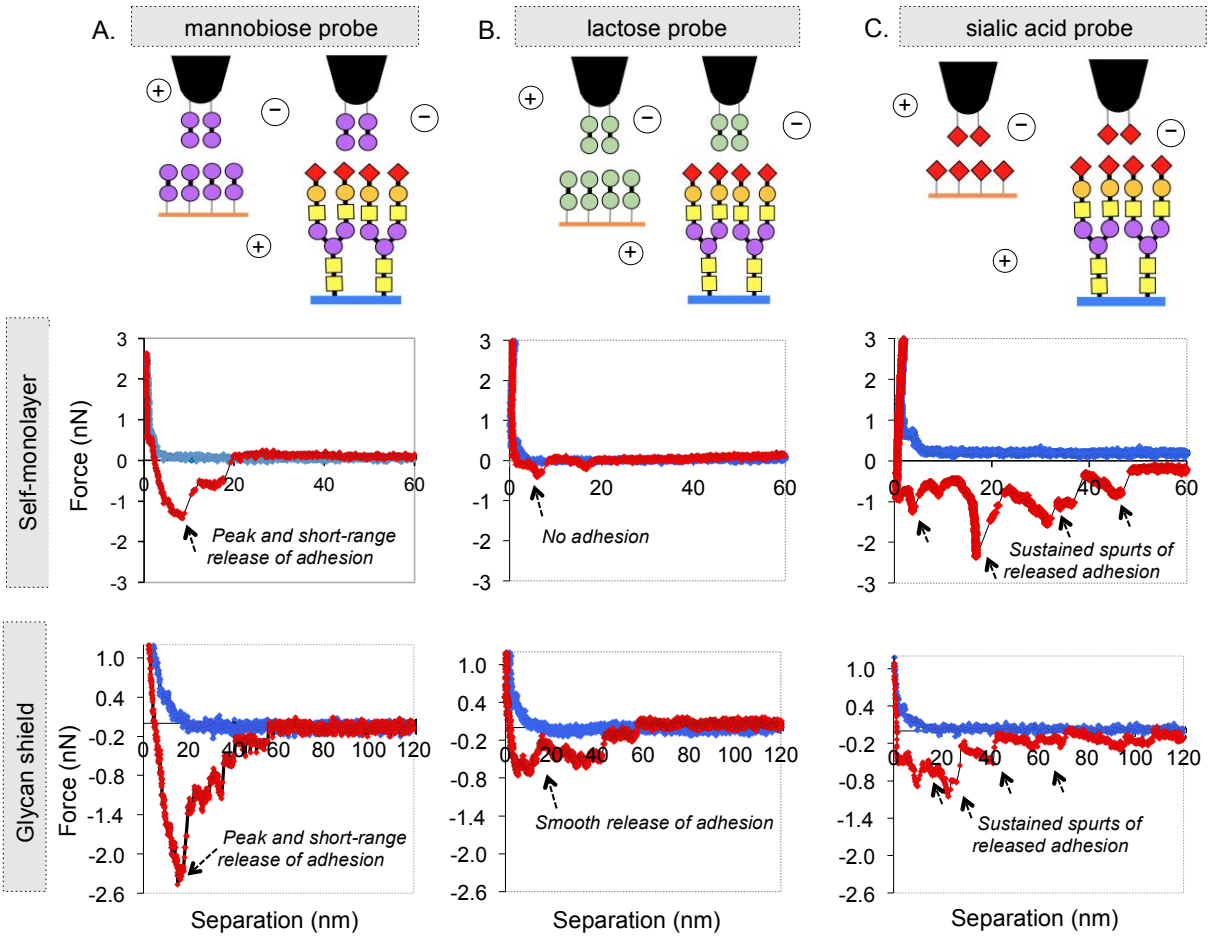

Figure 7: Interactions of a sugar-coated probe with the virus glycan shield and self-sugar monolayers in 150mM NaCl. Approach force curves are shown in blue and retraction curves are shown in red. (A) Depiction of a mannobiose-coated probe approaching a mannobiose monolayer and a virus glycan shield (top); and force curves resulting from probe interaction with the mannobiose monolayer (middle) and glycan shield (bottom). (B) Depiction of an SA-coated probe approaching a SA-monolayer and a virus glycan shield (top); and force curves resulting from probe interaction with SA monolayer (middle) and glycan shield (bottom). (C) Depiction of a lactose-coated probe approaching a lactose monolayer and a virus glycan shield (top); and force curves resulting from probe interaction with the lactose monolayer (middle) and glycan shield (bottom).

Interactions between SA probe and virus glycan shield resemble self-interactions between two SA monolayers: Consider a SA-coated probe approaching a glycan shield; the probe will first contact a layer of SA and sample the interactions typical of two opposing SA monolayers (schematized in top panel of Figs. 6C and 7C). Pure SA monolayers have a self-adhesion pattern that is distinctly different than the self-adhesion of two mannose monolayers. SA residues are negative-charged due to a deprotonated carboxylate group with pKa ~2.6 [58]. In

low salt condition, the interactions of two SA monolayers are dominated by the unscreened charge-repulsion between the two (Fig. 6C, middle): (i) the approach and retraction force curves overlap indicating that the two self-repelling SA tiers do not penetrate, (ii) the resistance to approach arises at separations far beyond physical contact indicating long-range charge-repulsion, and (iii) the absence of negative force during retraction indicates that the two self-repelling SA monolayers do not adhere. At 150mM NaCl, the interactions of two SA layers changes drastically as the charge repulsion between the layers is screened: (i) the approach and retraction force curves do not overlap indicating penetration, (ii) the long-range resistance to approach disappears consistent with the salt-screening of charge repulsion, and (iii) saw-tooth like negative forces appear during retraction indicating adhesion between the two surfaces (Fig. 7C, middle panel). In salt conditions, the SA-SA adhesion forces are released characteristically in multiple spurts with the magnitude of the release peaks not abating even as the separation between the surfaces increases. Such a pattern of saw-tooth release has been documented with other charged proteoglycans such as mucin that also contain SA [59]. When a SA probe approaches and retracts from the glycan shield, all characteristic features of the interaction between two SA monolayers is seen: long-range repulsion to approach that decreases with salt supplementation; lack of penetration between the self-repelling layers in low salt condition; and the appearance of saw tooth self-adhesion only upon salt supplementation (Figs. 6C and 7C, lower panel). The similarities between SA-SA and SA-glycan interactions suggest that the SA probe is largely sampling the surface tier of SA residues in the virus glycan shield. The inference is also consistent with the observation that force jumps and plateauing due to break-in and membrane-penetration events were significantly diminished when the virus was deep indented with SA probes (Fig. 4B). The charge-repulsion between the terminal SA layers on the shield could be preventing the approaching SA-probe from penetrating the glycan shield to reach the membrane, instead compressing the virus as a whole.

Tough and brittle interactions of glycan shield with SA- and mannobiose- surfaces:

Both mannobiose- and SA- coated probes appear to self-adhere with their respective sugar tier in the glycan shield. However, there are two important differences in their adherence pattern. First, the occurrence of mannobiose self-adhesion decreases with salt, whereas that of SA increases with salt. The opposite salt effect is reflected in the histograms describing the distribution of adhesion energies and peak forces for both probe-glycan (Figs. 8A,D and C,E) and probe-monolayer (see Suppl. Info. 2) studies. The observed salt dependence is consistent with mannobiose self-adhesion being driven by hydrogen bonding (which decreases with salt

ions) and the SA self-adhesion being driven by charge interaction (which increases with salts screening mutual repulsion). Secondly, while mannobiose self-adhesion is typically released in a single large peak over a short separation distance (Fig. 7A), SA self-adhesion is released in multiple peaks whose magnitudes can increase with separation and persist to separations 3 – 4 times larger than the contact distance between the monolayers (Fig. 7C). As per the histogram in Fig. 8D, the SA-glycan adhesion lengths reach up to ~340nm in the presence of salt, whereas the mannobiose-glycan adhesion lengths reach up to only ~40nm. The peak force is higher but the adhesion distance is smaller for mannobiose-glycan and mannobiose-mannobiose interactions, whereas the peak force is smaller and the adhesion distance is larger for SA-glycan and SA-SA interactions. In other words, even though the adhesion energies (i.e., force X distance) for SA- and mannobiose- interaction with the glycan shield are distributed similarly (Fig. 8D), the release of the former is more akin to the fracturing of a ‘tough’ and yielding material (long-range sustained release of energy), whereas the release of the latter is similar to the fracturing of a ‘brittle’ glassy material (short-range large release of energy).

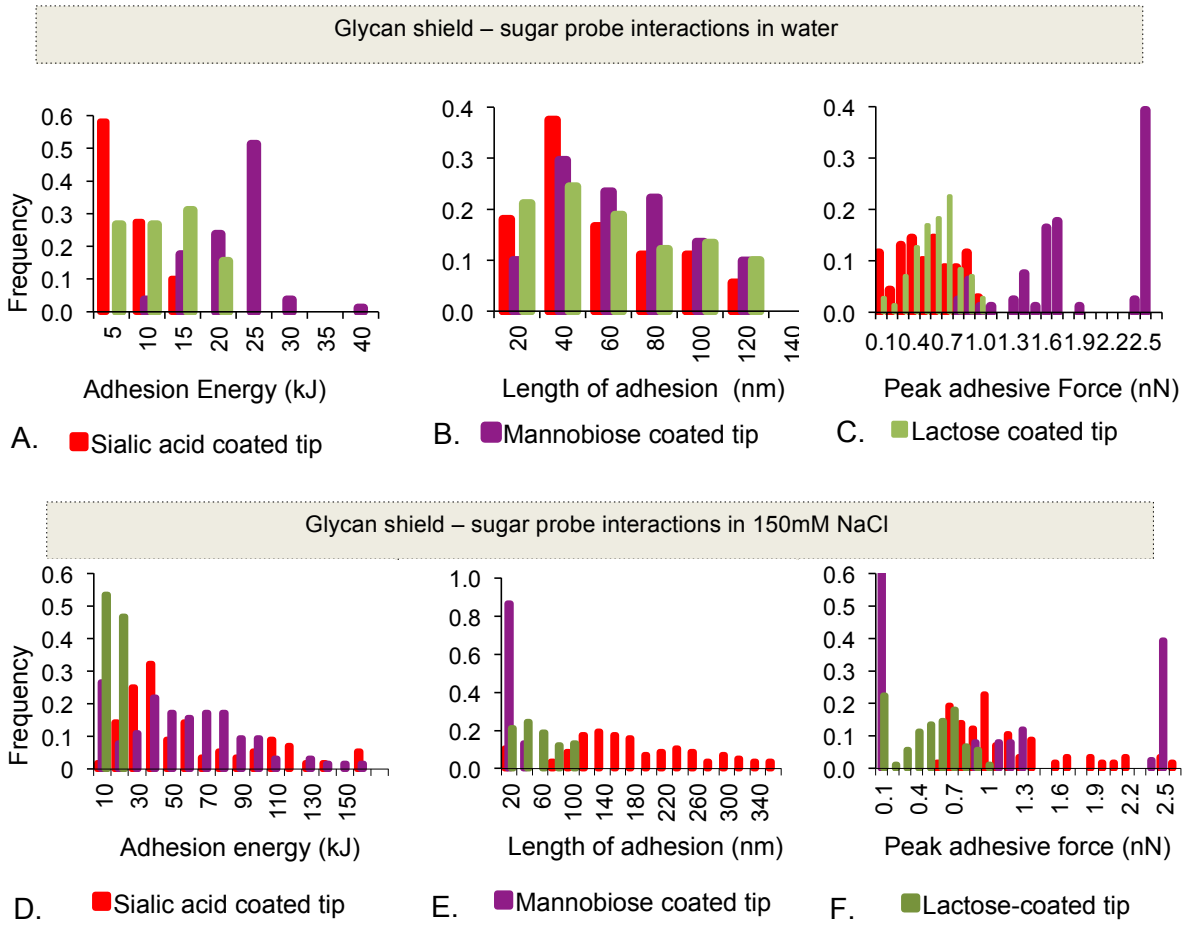

Fig. 8. Distribution of interaction features between sugar-coated AFM tips and virus glycan shield in 0mM and 150mM NaCl conditions (n > 100 force curves for each case).

Lactose residues possibly cross-interact with sialic acid monolayers/tiers of a glycan shield: Lactose is a disaccharide of glucose and galactose. While galactose per se is represented in the glycan shield, the lactose disaccharide can be tethered to the probe by its glucose or galactose end and therefore was presented as an ill-defined sugar control. As shown in Figs. 6B and 7B, the interactions of the lactose probe with the glycan shield were not similar to its interaction with an opposing lactose monolayer. Consider the interactions between two opposing lactose monolayers: At both 0 and 150mM NaCl, the monolayers do not self-penetrate (i.e., the approach and retraction curves overlap) and do not self-adhere (i.e., no negative forces during retraction) (see middle panels of Figs. 6B and 7B for probe-monolayer interaction force curves). However, negative forces of self-adhesion were observed when the lactose probe retracted from the glycan shield at both 0 and 150mM NaCl (see middle panels of Figs. 6B and 7B). Since SA is the first tier of sugars that the lactose probe will encounter on the glycan shield,

it is possible that the negative forces could results from strong cross-interactions between the lactose probes and the SA glycan tier, similar to those between the lactose probes and SA monolayers (Fig. 5B). While the source and implications of the interactions between lactose with SA/glycan-shield are not clear, they serve to highlight the unique design in the glycan shield where two predominantly positioned sugars, mannose and SA, not only do not cross-interact with each other but also possess distinct self-interactions patterns.

The control sugar-less probe coated with only the ATFMB linker molecules (that link sugar residues to the gold-lined surface of the probe tip) did not exhibit adhesive interactions with the virus glycan shield (Suppl. Info. 4A)

2B. Interactions in unenforced-contact conditions of solution studies.

It is not clear how the sugar-interaction patterns observed in the enforced-contact context of force spectroscopy apply to solution environments where the sugar-coated molecules and cells diffuse freely. In force spectroscopy, a mannobiose-coated tip can be forced into contact with the layer of mannose residues lying at the core of the glycan shield. But will the self-adhesions still manifest in an unenforced environment where superficial SA and galactose sugars can block access to the mannose core? Or would the diffusion energy from Brownian forces at room temperature be sufficient to overcome the hindrance posed? To investigate the self-interactions in an unenforced environment, we mixed virus particles with gold nanoparticles stabilized with citrate (control), lactose, mannobiose or SA. Since the hydrodynamic size of these nanoparticles (~10 - 20 nm) is much smaller than the size of the virus (~200 nm), the interaction scenario is more akin to viruses interacting with glycosylated macromolecules than with host cells. We note that the concentration of virus was maintained significantly lesser than the concentration of nanoparticles to prevent changes in solvent quality that would cause nanoparticles to self-aggregate. Also there was salt in the solution, which was necessary for keeping the gold nanoparticles dispersed.

Tracking strength and extend of binding with SPR shifts: Gold nanoparticle (np) solutions are red in color (Fig. 9A) and have a characteristic visible-range absorbance known as the surface plasmon resonance (SPR) [60]. The electrons of metallic nps are excited by light into a conduction band over the particle surface, which then oscillates with the electromagnetic field of the impinging light. The absorption peak shifts to longer wavelengths (i.e., the solution looks bluer) and broadens when either the size of nps increases (which is not applicable in our case);

or when the distance between nps decreases due to nps aggregating (among themselves or with viruses); or when moieties coat the nps surfaces (such as when nps adsorb on virus surfaces) [60-63]. The magnitude of the wavelength-shifts increases with the thickness of the layer adsorbed on the np surface [64].

When a small amount of virus (10 µl of 1:100 dil. of $1x10^7$ / ml viral titers) was added to mannobiose- and lactose- coated nanoparticles, the solutions turned blue (Fig. 9A). The primary SPR peak for mannobiose-probes was blue-shifted 10nm from the original peak, whereas that for lactose-probes was shifted only 4nm (Table 1). An SPR shift of this modest size can be attributed to nps binding on or coating the virus, and the mannobiose probes bind stronger than lactose ones. When virus was added to SA-coated nps, the solution turned blue and precipitates were observed. The primary peak was shifted by 85nm and broad, suggesting that the SA probes were fostering large-scale aggregation events involving multiple viruses and of varying size (Fig. 9A, Table 1). There was also a smaller secondary peak having the same absorption wavelength as plain SA np solutions (i.e., 0nm shift). It can be attributed to the free SA-nps not involved in the large-scale aggregation with virus (Fig. 9B).

Tracking size of diffusing entity with DLS: Dynamic Light Scattering can be used to further interrogate how the probes bind or aggregate virus by tracking changes in the size of the diffusing species (Fig. 9C). The D_H of the sugar-coated nps falls in the 10 – 20nm range, whereas that of the virus is ~200nm (listed in Table 1). When virus is added to mannobiose- and lactose- nps, the correlation curves shift slightly to the right, as the D_H increases to ~365nm and ~380 nm, respectively. These hydrodynamic sizes are modestly larger than the size of the virus, and consistent with nps coating the virus, but with the mannobiose-probes coating more deeply into the virus (smaller D_H increase). When virus was added to SA-nps, the correlation curves had larger shifts to the right (Fig. 9C), with the D_H of the diffusing species reaching 500 nm and ~0.1 microns (Table 1). The large aggregation of virus and SA probes observed in DLS is consistent with the large SPR shifts measured for the solution, and the occurrence of precipitation in the cuvettes.

Unenforced virus interactions of sugar-probes reflect differences in force-spectroscopy. Consider how the probes will interact with virus in solution based on the findings from the enforced contact environment of force-spectroscopy. The mannobiose-probe will reach the mannose-core of the glycan shield unhindered, latching deep within the shield (depicted in Fig

9D, left). On the other hand, the lactose-probe will bind to the SA residues on the surface of the glycan shield (depicted in Fig 9D, middle). The SPR and DLS shifts for lactose- and mannobiose- probes are consistent with the above picture of nps coating the surface of the virus. Within these two shifts, the larger SPR but smaller DLS shifts for viruses bound with mannobiose-nps are consistent with the idea of these nps binding tighter and deeper on the virus. AFM phase images of the surface-dried virus+mannobiose-np aggregates show smooth particles that are ~40nm high and taller than uncoated virus (Fig. 9D, left), having well-defined borders that are not distorted by the surface adsorption and drying occurring during sample preparation. In contrast, the surface-dried virus+lactose-nps aggregates were disordered, consistent with surface adhesion of nps being distorted by the conditions of sample preparation (Fig. 9D, middle). Similarly, the differences between the virus binding of mannobiose- and SA-probes reflect the 'brittle', short-range and 'tough' long-range interactions implied by force spectroscopy. The mannobiose-nps form tight coats on viruses consistent with the short-range nature of the adhesion release from the glycan shield, whereas SA-nps form large aggregates consistent with the long-range and yielding nature of their adhesion release from the glycan surface (Fig. 9D, right)

The control solution where virus was added to plain citrate-stabilized nps did not show any indication of nps coating or aggregating the virus; there was no change in solution color, no shifts in the SPR absorption spectrum, and no D_H increase from a diffusing species larger than the virus (Suppl. Info. 4B).

A.

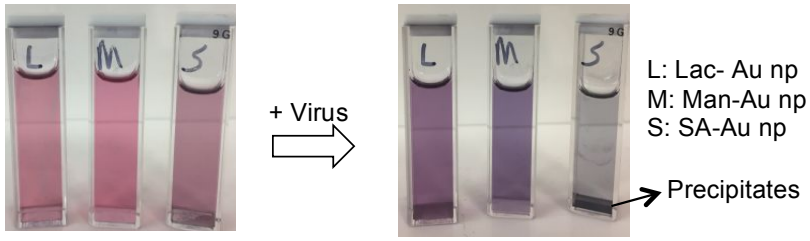
L
M
S
+ Virus
L
M
S
L: Lac- Au np
M: Man-Au np
S: SA-Au np
Precipitates

B.

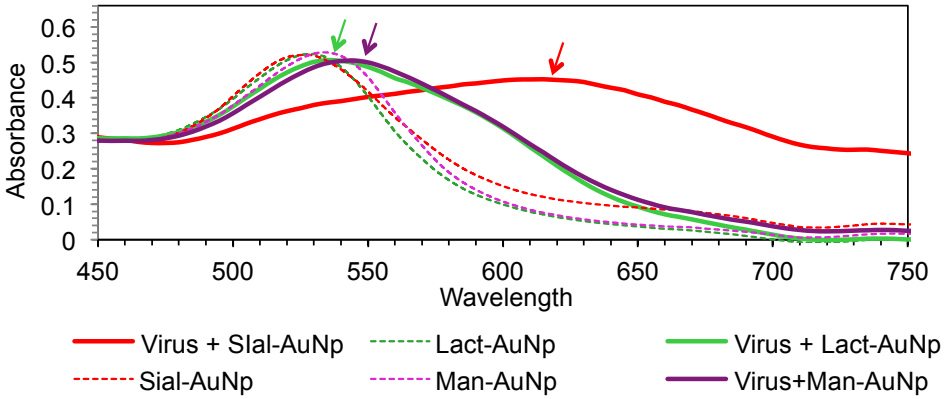
Absorbance
0.6
0.5
0.4
0.3
0.2
0.1
0
450
500
550
600
650
700
750
Wavelength
Virus + SIal-AuNp
Lact-AuNp
Virus + Lact-AuNp
Sial-AuNp
Man-AuNp
Virus+Man-AuNp

C.

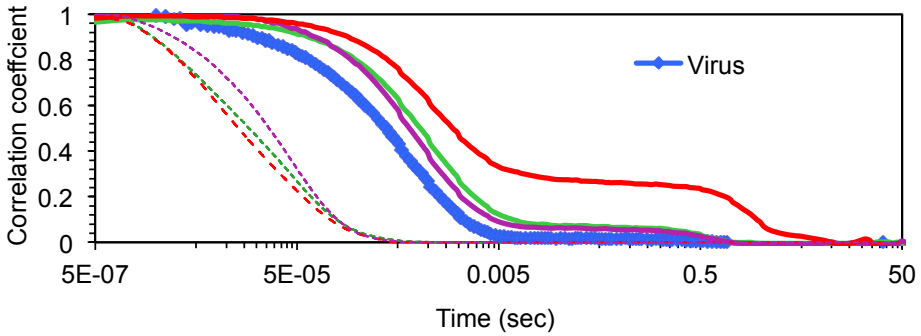
Correlation coeffcient
1
0.8
0.6
0.4
0.2
0
5E-07
5E-05
0.005
0.5
50
Time (sec)
Virus

D.

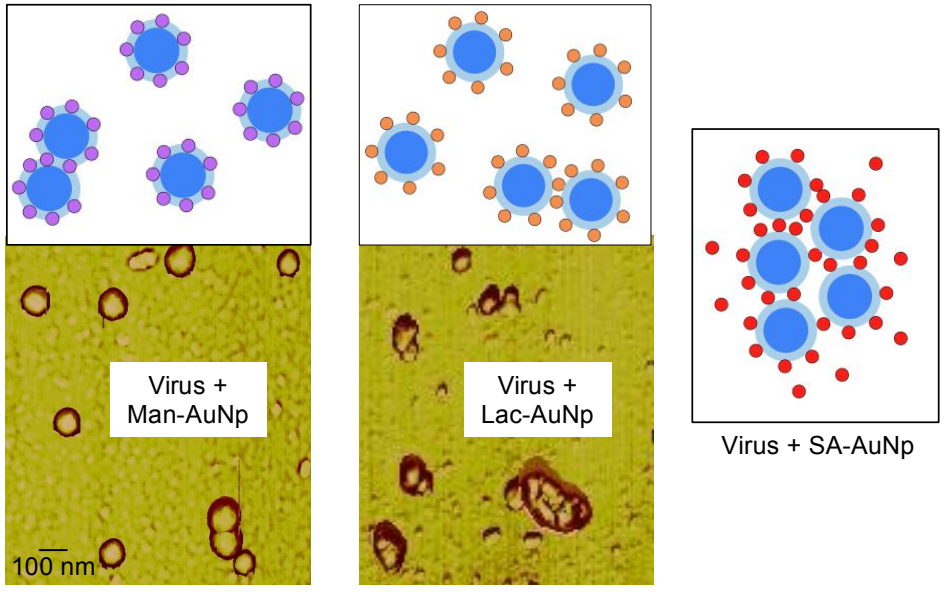
Virus +
Man-AuNp
Virus +
Lac-AuNp
Virus + SA-AuNp
100 nm

Fig.9: Interaction between sugar-stabilized gold nanoparticles and virus suspensions. (A) Solutions of mannobiose 'M', Lactose 'L', and sialic acid 'S' stabilized gold nanoparticles underwent a color change from red to shades of blue when 10µl of 1:100 dil of $1x10^9$ viral titer was added to the mix. SA-nps + virus solution had precipitates. (B) Surface plasmon resonance (visible range absorbance) spectrum of lactose-, mannobiose- and sialic acid- stabilized gold nanoparticles (in dotted lines), and the shifts observed when viral particles were added to the nanoparticle solution (solid lines). The shifted peak wavelengths are pointed out in the Figure. SA-nps + virus solutions has significant shifts, whereas mannobiose- and lactose- nps had modest shifts with the former larger than the latter. (C) DLS correlation curves from sugar-stabilized nanoparticles before and after virus addition. SA-nps + virus solutions showed large increases in D_H (rightward shift of exponential falls), whereas lactose- and mannobiose- nps + virus solutions showed modest increases with the former slightly larger than the latter. (D) The left image is a pictorial representation of mannobiose-nps binding to the mannose core deep into the glycan shield (depicted by the light blue halo around the blue virus particle), with AFM phase images showing the bound virus particles to be well-defined and ordered. The middle image is a pictorial representation of lactose-nps binding to the SA surface of the glycan shield of viruses, with the associated AFM phase images suggesting loose and disordered binding between the virus and the nps. The right is a pictorial representation of the large aggregates formed by SA-np binding to the SA-surface of the glycan in long-range adhesions.

	SPR (nm) [$]	+ virus SPR (nm) [$]	D_H (nm) [$]	+ virus D_H (nm)[$]
Mannobiose-stabilized nps	520	610, 525	13.2 ± 0.1	304 ± 16.9
Lactose-stabilized nps	535	545	10.1±1.7	357 ±15.2
SA-stabilized nps	534	530	4.8± 0.7	482 ±10.7; 1000
Citrate-stabilized nps (control)	525	520	22.9 ± 0.12	55 ± 1.8

[$] should be compared against D_H of Virus suspensions, ~200 nm.

Table 1: Summary of SPR and DLS readings for virus binding with different sugar-stabilized gold nanoparticles.

DISCUSSION

In this study, we surveyed the structure of a replication-deficient HIV-1 pseudovirus and probed carbohydrate interactions with the virus glycan shield. Our main findings are discussed below.

Organization of VSV-G pseudotyped HIV-1 virus: The model organism in this study is the pseudovirus HIV-1 R^- E^- / VSV-G. It is deficient in the accessory proteins that control viral replication and virulence, and in the *env* gene that produces the HIV-1 transmembrane protein gp120. Instead, the virus is pseudotyped with the glycoproteins from the vascular stomatitis virus (VSV). The pseudovirus is widely used in research due to its deficiency in replication and associated low disease risk [32]. Overall the structure, size, and shape of the pseudovirus are consistent with those described for the wild-type HIV-1 virus (Suppl. Info. 1). The images of surface-adsorbed and air-dried pseudovirus support another report of a multiple-capsid sub-population in wild-type HIV-1 virus [49]. The hydrodynamic diameter of the pseudovirus is about 2X the air-dried surface diameter, and could be attributed to the presence of a swollen glycan shield and membrane in solution. When indented with a bare AFM tip, virus resistance to an approaching tip can be summarized in three regimes, where the tip (i) penetrates a glycan-shield, (ii) breaks through to penetrate and buckle the membrane envelope, and (iii) indents and penetrates a hard capsid. Overall the virus and capsid appear collapsed on the surface for the particular case of pseudotyping and testing conditions. The HIV capsid is known to undergo a 'stiffness switch' during maturation, in which a hard capsid becomes malleable, and which is essential for the virus infectivity [43, 65, 66]. In a nano-indentation experiment of a virus with a glycan shield, the initial resistance encountered by an AFM probe could come from penetrating the glycan shield, which then may not be an estimate of the compression resistance of the whole virus.

Access and latching to mannose core are unhindered by the distal residues: All N-glycosylated glycans have a core of mannose residues to which distal sugars may be added [3, 7]. Our study shows that there is no significant cross-interaction between mannose and the sugars distal to it (SA and galactose); and that a mannobiose- coated probe could access the mannose residues underneath the layers of acetyl glucosamine, galactose, and sialic acid to produce a self-adhesion pattern similar to two pure mannobiose monolayers adhering [11]. As a mannobiose-coated probe traverses the glycan shield in deep-indentation experiments, brief regions of force falls were observed, that were reminiscent of the break-through forces seen

between two pure mannobiose layers. Also, when a mannobiose-coated probe retracts after contacting the mannose core, the adhesion is relieved quickly in a peak negative force close to the surface. The pattern of release is similar to how adhesion is released between two pure mannobiose monolayers, and is distinctively different from other sugar-adhesion release patterns. The findings raise questions about the choice and placement of sugars in the glycan shield, and if they were evolutionarily favored to facilitate access to the mannose core?

Tough long-range and brittle short-range sugar interactions in biological carbohydrate covers: Both mannose and SA are common surface sugars in eukaryotes. In addition, mannose is present universally at the core of all N-glycan sugars. SA abounds on the surface of cancer cells [3, 7]. We found that both sugars exhibit self-adhesion, but are different in their fundamental governing force. The self-adhesion of mannose residues involves hydrogen-bonding interactions, relies on spatial proximity of residues, gets maximally released at inter-surface pull out, and is attenuated by salt. The self-adhesion of SA residues involves long-range like-charge attractions and gets stronger as surfaces are pulled apart, gets released in multiple steps over long distances, and is enhanced by salt in the medium. In solution, these different self-adhesion patterns cause mannose-coated nps to coat complex-type glycan shield, but SA-coated nps to aggregate the same complex-type virus shields. The consistency between the enforced surface and the unenforced solution interactions rule out the possibility that the long-range SA self-interactions was due to the SA monolayer peeling of the AFM probes. From a material-science standpoint, biological surfaces brought together by mannose interactions would behave like brittle and unyielding material (i.e., strong and hard, but will break completely once the force or strain exceeds a point), whereas biological surfaces brought together by SA interactions would behave more like a plastic and yielding material whose overall strength is low but can be sustained even after fracture over a long strain distance.

The differences in the self-adhesion behavior of SA-SA and mannobiose-mannobiose residues can be explained by the different underlying sources of their adhesion. Mannobiose-mannobiose adhesion is driven by hydrogen bonding between the mannobiose residues, which explains the existence of a break-in force (to break hydrogen bonds within a monolayer and reform them with the penetrating layer), peak release of self-adhesion at the interface of retracting monolayers (when penetrated monolayers of mannose break ‘out’), and increase in occurrence of non-adhesion with salt ions (diffusing salt ions interfere with formation of stable hydrogen-bond networks). The self-adhesion between SA-SA residues on the other hand

appears to be governed by the phenomena of long-range attraction between like-charged bodies in a salt medium [67, 68]. These attraction forces occur as counter-ions layer on a charged surface and invert the surface charge locally, resulting in opposing like-charged surfaces to attract [67, 69, 70]. A similar phenomenon is responsible for negative-charged strands of DNA being attracted to each other and compacting in the presence of multivalent ions [71]. These attractive forces between like-charged surfaces occur when the surface charge is effectively neutralized by salt ions (i.e., no long-range resistance to the approach of like-charged surfaces), and tend to increase as the surfaces move apart till an optimal separation is reached [72, 73]. The sialic-sialic self-adhesions showed all these features. Also, as expected, because of the different physics underlying their self-interactions, opposing layers of mannose and sialic acid did not exhibit cross-adhesion in both water and salt medium.

Lactose and SA surfaces cross-interact: Though lactose is a diastereomer of mannobiose, lactose-lactose and lactose-mannose residues do not adhere in both 0 and 150mM NaCl. Lactose and mannose residues differ in the type of glycosidic linkages and in the positioning of the hydroxyl groups on the second and fourth carbons of each ring. The structural differences may alter the pattern of hydrogen-bonding and occurrence of self-adhesion behavior. Lactose is not present per se in the glycan shields of viruses, but its constituent residue galactose is present beneath the SA surface of the shield [7]. Unexpectedly we observed strong adhesion between lactose-probes and SA monolayer in both 0 and 150mM NaCl. We observed similar adhesion between lactose-probes and the glycan shield, which has a surface layer of SA residues. The retraction forces did not have the single peak character of mannobiose-mannobiose adhesion release, or the multi-peak character of SA-SA adhesion release. In several cases we found the negative force curves to change smoothly without sharp jumps, suggesting more so an entanglement-like adhesion than sharp breakage of strong bonds. The mechanism by which a charged surface such as SA would adhere to an uncharged surface such as lactose is not clear.

A summary of the sugar-interaction findings is presented in Table 2. The study suggests that the pattern of sugar placement in the glycan shield may have evolved to guide specific adherence patterns for carbohydrate covers, irrespective of receptor-mediated interactions (Table 2). The findings imply how different types of carbohydrate covers would adhere: two high-mannose carbohydrate cover would have strong self-latching interactions throughout the glycan shield; a high-mannose and complex-type shield could latch strongly at the mannose core; and two

complex-type carbohydrate covers could adhere in reformable interactions at the surface. The findings of this study can be summarized by the principle that the complex-type N glycan shield will adhere to a sugar probe with the pattern of its most superficial sugar tier capable of adhering to the sugar probe (Table 2). These principles can also guide the design of drug and DNA delivery vehicles based on the carbohydrate cover of the target cells.

	Sialic acid monolayer	Lactose monolayer	Mannose monolayer	Complex N-Glycan shield
Sialic acid probe	Long-range charge-mediated adhesion 'tough'	Adhesion	Negligible	Long-range charge-mediated adhesion 'tough'
Lactose probe	Adhesion	No self-adhesion	Negligible	Unorganized adhesion
Mannose probe	Negligible	Negligible	Short-range H-bond mediated adhesion 'brittle'	Short-range H-bond mediated adhesion 'brittle'

Table 2: Summary of the interactions between sugar probes and respective sugar monolayers and the N-glycan shield of complex type. The interactions of the glycan shield, which is a composite of the above sugar layers with SA being the distal most and galactose being present instead of lactose, can be deconvoluted to arise from its most superficial layer that can adhere with the sugar on the approaching probe.

In our study, the sugars were attached to linkers assembled on the probe using aryl-azide based photochemistry. Upon UV exposure, the azide head group on ATFMB linkers converts into a reactive nitrene group, which inserts into the C-H bonds of the sugar.[74, 75] Since it is not possible to control where the insertion occurs, the method presents an assorted orientation of interaction faces. Our study findings warrant future work with more controlled presentation of sugars [76, 77]. However we do note that unlike sugar-lectin interactions where the sugar has to dock within a relatively-inflexible ligand-binding pocket on proteins, sugar-sugar interactions are between two flexibly-presented entities and therefore the interactions can be expected to be less dependent on sugar presentation compared to sugar-protein interactions.

In this study, the force spectroscopy was performed in water, with and without salt supplementation, to identify the sugar tier and mechanism mediating glycan adhesion by amplifying conditions that foster either hydrogen bonding or charge interactions. Our central finding is that the adhesion of a complex glycan shield can be deconvoluted to brittle mannose and tough SA self-adhesions, but due to the ionic dependence of hydrogen-bonding and charge- interactions, we expect the manifestation of mannose and SA self-adhesions to change

with the ionic strength and ion valence in the medium. Also, to control the salt concentration, separate buffering agents were not added during force spectroscopy. The pH of CO_2-buffered salt solution in our experiments is ~6. SA is the only protonable sugar in the N-glycans on VSV G proteins, but it has a pKa of ~2 well below our operating pH. Therefore we do not expect the operating pH to alter the physiological relevance of our findings as far as the glycan interactions are concerned. As for the pH stability of the virus protein and lipid assembly presenting the glycans, we note that when the VSV-G pseudotyped HIV infects a cell, it is trafficked through endosomal vesicles like the native VSV virus, before the capsid is released into the cytoplasm.[33] In other words the VSV-G pseudotyped HIV can survive the low pH conditions within endosomes. Moreover HIV lipid membrane is reported to be stable for several hours between pH 3 and 10.[78] Therefore we do not expect the virus macromolecular structure presenting the glycans to disintegrate at the operating pH in the time-span of the experiments. The VSV G protein, however, does change conformation below pH 6 to expose domains that help the virus fuse with the endosome membrane. [79, 80]

CONCLUSION:

The pattern of glycosylation in VSV-G proteins have several features representative of the diverse class of N-linked complex-type glycans: (i) the mannose-core structure is conserved in N-linked glycoproteins from viruses to bacteria to mammalian cells [3, 37, 81], (ii) sialic-acid is one of the most prevalent terminal residues and is involved in binding host-receptors and membrane [3, 38, 82], and (iii) it is common for complex-type glycans to have one or more repeats of N-acetyl glucosamine and galactose between the core and the terminal residue [3, 9]. In five different experimental setups, we observed a consistent portrayal of mannose-mannose and SA-SA self-interactions as ‘brittle’ and ‘tough’ adhesions, respectively, that were not significantly inhibited by cross-interactions. The study suggests that there are well-defined interaction contributions from the individual sugars of an archetypal N-glycan; and that the interaction of a sugar probe with the glycan shield, and possibly between different glycan shields themselves, can be derived from the individual sugar interactions (Table 2).

AKNOWLEDGEMENTS:

We are very grateful to Dr. Byrnes for insightful comments on the research and manuscript. We are also thankful to Dr. J.W. Mitchell for access to the Nanomaterials lab at Howard University,

and to lab managers Mr. James Griffin, Mr. Crawford Taylor and Mr. Anthony Gomez. We thank Dr. Sergei Nekhai and Dr. Namita Kumari for supplying virus solutions and for discussions on virus stability, undergraduate students Ms. Wintana Teowolde and Ms. Aliyah Godwin for assistance with data analysis; Drs. Anna Allen for commenting on the manuscript, and Dr. Saswati Basu for discussions. The work was supported by the National Science Foundation under grant no. 1407891 awarded to Preethi Chandran.

Conflicts of interest: None

REFERENCES

1. A. Driouich, P. Gonnet, M. Makkie, A.-C. Laine and L. Faye, *Planta*, 1989, **180**, 96.
2. M. Treuheit, C. Costello and T. Kirley, *Journal of Biological Chemistry*, 1993, **268**, 13914-13919.
3. D. J. Vigerust and V. L. Shepherd, *Trends in Microbiology*, 2007, **15**, 211-218.
4. J. Balzarini, K. Van Laethem, S. Hatse, M. Froeyen, W. Peumans, E. Van Damme and D. Schols, *Journal of Biological Chemistry*, 2005, **280**, 41005-41014.
5. L. Cao, J. K. Diedrich, D. W. Kulp, M. Pauthner, L. He, S. R. Park, D. Sok, C. Y. Su, C. M. Delahunty, S. Menis, R. Andrabi, J. Guenaga, E. Georgeson, M. Kubitz, Y. Adachi, D. R. Burton, W. R. Schief, J. R. Yates Iii and J. C. Paulson, *Nat Commun*, 2017, **8**, 14954.
6. U. Rathore, P. Saha, S. Kesavardhana, A. A. Kumar, R. Datta, S. Devanarayanan, R. Das, J. R. Mascola and R. Varadarajan, *Journal of Biological Chemistry*, 2017, **292**, 10197-10219.
7. D. J. Vigerust, K. B. Ulett, K. L. Boyd, J. Madsen, S. Hawgood and J. A. McCullers, *Journal of virology*, 2007, **81**, 8593-8600.
8. J. J. Lyons, J. D. Milner and S. D. Rosenzweig, *Frontiers in Pediatrics*, 2015, **3**.
9. E. Bieberich, *Advances in neurobiology*, 2014, **9**, 47-70.
10. M. A. Robertson, J. R. Etchison, J. S. Robertson, D. F. Summers and P. Stanley, *Cell*, 1978, **13**, 515-526.
11. H. K. Abeyratne-Perera and P. L. Chandran, *Langmuir*, 2017, **33**, 9178-9189.
12. A. Carvalho de Souza and J. P. Kamerling, in *Methods in Enzymology*, ed. F. Minoru, Academic Press, 2006, vol. Volume 417, pp. 221-243.
13. I. Bucior, S. Scheuring, A. Engel and M. M. Burger, *J Cell Biol*, 2004, **165**, 529-537.
14. L. Cui, K. Johkura, F. Yue, N. Ogiwara, Y. Okouchi, K. Asanuma and K. Sasaki, *Journal of Histochemistry & Cytochemistry*, 2004, **52**, 1447-1457.
15. Y. Song, D. A. Withers and S.-i. Hakomori, *Journal of Biological Chemistry*, 1998, **273**, 2517-2525.
16. S.-i. Hakomori, *Pure and applied chemistry*, 1991, **63**, 473-482.
17. D. Spillmann, *Glycoconjugate J*, 1994, **11**, 169-171.
18. X. Fernàndez-Busquets, A. Körnig, I. Bucior, M. M. Burger and D. Anselmetti, *Molecular Biology and Evolution*, 2009, **26**, 2551-2561.
19. S. Garcia-Manyes, I. Bucior, R. Ros, D. Anselmetti, F. Sanz, M. M. Burger and X. Fernàndez-Busquets, *Journal of Biological Chemistry*, 2006, **281**, 5992-5999.
20. B. Lorenz, L. Álvarez de Cienfuegos, M. Oelkers, E. Kriemen, C. Brand, M. Stephan, E. Sunnick, D. Yüksel, V. Kalsani, K. Kumar, D. B. Werz and A. Janshoff, *Journal of the American Chemical Society*, 2012, **134**, 3326-3329.
21. S. R. Haseley, H. J. Vermeer, J. P. Kamerling and J. F. G. Vliegenthart, *Proceedings of the National Academy of Sciences*, 2001, **98**, 9419-9424.
22. E. Stansell and R. C. Desrosiers, *The Yale journal of biology and medicine*, 2010, **83**, 201.
23. W. Van Breedam, S. Pöhlmann, H. W. Favoreel, R. J. de Groot and H. J. Nauwynck, *FEMS Microbiology Reviews*, 2014, **38**, 598-632.
24. L. Ehrlich, S. Fong, S. Scarlata, G. Zybarth and C. Carter, *Biochemistry*, 1996, **35**, 3933-3943.
25. I. Tabas, S. Schlesinger and S. Kornfeld, *Journal of Biological Chemistry*, 1978, **253**, 716-722.

26. S. Charles, T. Ammosova, J. Cardenas, A. Foster, J. Rotimi, M. Jerebtsova, A. A. Ayodeji, X. Niu, P. E. Ray, V. R. Gordeuk, F. Kashanchi and S. Nekhai, *Journal of cellular physiology*, 2009, **221**, 469-479.
27. E. Le Rouzic and S. Benichou, *Retrovirology*, 2005, **2**, 11.
28. J. L. Foster and J. V. Garcia, *Retrovirology*, 2008, **5**, 84.
29. R. Benson, A. Sanfridson, J. Ottinger, C. Doyle and B. Cullen, *Journal of Experimental Medicine*, 1993, **177**, 1561-1566.
30. P. S. Linsley, J. A. Ledbetter, E. Kinney-Thomas and S. Hu, *Journal of virology*, 1988, **62**, 3695-3702.
31. D. Finkelshtein, A. Werman, D. Novick, S. Barak and M. Rubinstein, *Proceedings of the National Academy of Sciences*, 2013, **110**, 7306-7311.
32. F. Y. Tung, C. R. Rinaldo, Jr. and R. C. Montelaro, *AIDS Res Hum Retroviruses*, 1998, **14**, 1247-1252.
33. C. Aiken, *Journal of Virology*, 1997, **71**, 5871-5877.
34. A. Engelman and P. Cherepanov, *Nature reviews. Microbiology*, 2012, **10**, 279-290.
35. L. Deshmukh, C. D. Schwieters, A. Grishaev, R. Ghirlando, J. L. Baber and G. M. Clore, *Journal of the American Chemical Society*, 2013, **135**, 16133-16147.
36. B. Grigorov, D. Décimo, F. Smagulova, C. Péchoux, M. Mougel, D. Muriaux and J.-L. Darlix, *Retrovirology*, 2007, **4**, 54.
37. J. R. Etchison and J. J. Holland, *Proceedings of the National Academy of Sciences*, 1974, **71**, 4011-4014.
38. C. L. Reading, E. E. Penhoet and C. E. Ballou, *Journal of Biological Chemistry*, 1978, **253**, 5600-5612.
39. G. J. Kotwal, M. L. Buller, W. H. Wunner, C. R. Pringle and H. P. Ghosh, *Journal of Biological Chemistry*, 1986, **261**, 8936-8943.
40. D. C. Klein, C. M. Stroh, H. Jensenius, M. van Es, A. Kamruzzahan, A. Stamouli, H. J. Gruber, T. H. Oosterkamp and P. Hinterdorfer, *ChemPhysChem*, 2003, **4**, 1367-1371.
41. K. A. Curtis, D. Miller, P. Millard, S. Basu, F. Horkay and P. L. Chandran, *PLoS ONE*, 2016, **11**, e0158147.
42. R. Ramalho, S. Rankovic, J. Zhou, C. Aiken and I. Rousso, *Retrovirology*, 2016, **13**, 17.
43. N. Kol, Y. Shi, M. Tsvitov, D. Barlam, R. Z. Shneck, M. S. Kay and I. Rousso, *Biophysical journal*, 2007, **92**, 1777-1783.
44. K. Soo-hyun and L. and Kwang-il, *Mol. Cells*, 2017, **40**, 339-345.
45. F. Higashikawa and L.-J. Chang, *Virology*, 2001, **280**, 124-131.
46. W. Lucas, in *eLS*, John Wiley & Sons, Ltd, 2001.
47. I. A. T. Schaap, F. Eghiaian, A. des Georges and C. Veigel, *The Journal of Biological Chemistry*, 2012, **287**, 41078-41088.
48. Matthew R. Angle, A. Wang, A. Thomas, Andreas T. Schaefer and Nicholas A. Melosh, *Biophysical Journal*, 2014, **107**, 2091-2100.
49. G. A. Frank, K. Narayan, J. W. Bess, Jr., G. Q. Del Prete, X. Wu, A. Moran, L. M. Hartnell, L. A. Earl, J. D. Lifson and S. Subramaniam, *Nat Commun*, 2015, **6**, 5854.
50. N. Arhel, *Retrovirology*, 2010, **7**, 96.
51. M. G. Mateu, *FEBS Journal*, 2009, **276**, 6098-6109.
52. L. A. Alcaraz, M. del Álamo, F. N. Barrera, M. G. Mateu and J. L. Neira, *Biophysical Journal*, 2007, **93**, 1264-1276.

53. O. Pornillos, B. K. Ganser-Pornillos, B. N. Kelly, Y. Hua, F. G. Whitby, C. D. Stout, W. I. Sundquist, C. P. Hill and M. Yeager, *Cell*, 2009, **137**, 1282-1292.
54. A. T. Gres, K. A. Kirby, V. N. KewalRamani, J. J. Tanner, O. Pornillos and S. G. Sarafianos, *Science (New York, N.Y.)*, 2015, **349**, 99-103.
55. M. L. Oyen, *Current Opinion in Solid State and Materials Science*, 2015, **19**, 317-323.
56. Y. Zhu, Z. Dong, U. C. Wejinya, S. Jin and K. Ye, *Journal of biomechanics*, 2011, **44**, 2356-2361.
57. H. Takahashi, *Anatomy and embryology*, 1992, **185**, 389-400.
58. E. R. Vimr, K. A. Kalivoda, E. L. Deszo and S. M. Steenbergen, *Microbiology and Molecular Biology Reviews*, 2004, **68**, 132-153.
59. M. Sumarokova, J. Iturri, A. Weber, M. Maares, C. Keil, H. Haase and J. L. Toca-Herrera, *Scientific Reports*, 2018, **8**, 9660.
60. C. Lee, M. A. Gaston, A. A. Weiss and P. Zhang, *Biosensors and Bioelectronics*, 2013, **42**, 236-241.
61. Z. Zhong, S. Patskovskyy, P. Bouvrette, J. H. Luong and A. Gedanken, *The Journal of Physical Chemistry B*, 2004, **108**, 4046-4052.
62. C. D. Medley, J. E. Smith, Z. Tang, Y. Wu, S. Bamrungsap and W. Tan, *Analytical chemistry*, 2008, **80**, 1067-1072.
63. J. J. Storhoff, S. S. Marla, P. Bao, S. Hagenow, H. Mehta, A. Lucas, V. Garimella, T. Patno, W. Buckingham and W. Cork, *Biosensors and Bioelectronics*, 2004, **19**, 875-883.
64. K.-L. Lee, C.-C. Chang, M.-L. You, M.-Y. Pan and P.-K. Wei, *Scientific reports*, 2016, **6**, 33126.
65. J. Coffin, Cold Spring Harbor (NY), 1997.
66. H.-B. Pang, L. Hevroni, N. Kol, D. M. Eckert, M. Tsvitov, M. S. Kay and I. Rousso, *Retrovirology*, 2013, **10**, 4.
67. J. E. Sader and D. Y. Chan, Elsevier, 1999.
68. T. E. Angelini, H. Liang, W. Wriggers and G. C. Wong, *Proceedings of the National Academy of Sciences*, 2003, **100**, 8634-8637.
69. J. Piñero, L. B. Bhuiyan, J. Reščič and V. Vlachy, *The Journal of Chemical Physics*, 2007, **127**, 104904.
70. G. S. Manning, *Quarterly Reviews of Biophysics*, 2009, **11**, 179-246.
71. M. Gebala, G. M. Giambaşu, J. Lipfert, N. Bisaria, S. Bonilla, G. Li, D. M. York and D. Herschlag, *Journal of the American Chemical Society*, 2015, **137**, 14705-14715.
72. M. B. McBride and P. Baveye, *Soil Science Society of America Journal*, 2002, **66**, 1207-1217.
73. P. Kékicheff and O. Spalla, *Physical review letters*, 1995, **75**, 1851.
74. C. Madwar, W. Chu Kwan, L. Deng, O. Ramström, R. Schmidt, S. Zou and L. A. Cuccia, *Langmuir*, 2010, **26**, 16677-16680.
75. X. Wang, O. Ramström and M. Yan, *Journal of materials chemistry*, 2009, **19**, 8944-8949.
76. X.-L. Sun, C. L. Stabler, C. S. Cazalis and E. L. Chaikof, *Bioconjugate Chemistry*, 2006, **17**, 52-57.
77. J. K. Bhattarai, D. Neupane, V. Mikhaylov, A. V. Demchenko and K. J. Stine, in *Carbohydrate*, InTech, 2017.

78. S. A. o. P. T. b. B. German Advisory Committee Blood, *Transfusion medicine and hemotherapy : offizielles Organ der Deutschen Gesellschaft fur Transfusionsmedizin und Immunhamatologie*, 2016, **43**, 203-222.
79. P. Rücker, S. A. Wieninger, G. M. Ullmann and H. Sticht, *Proteins: Structure, Function, and Bioinformatics*, 2012, **80**, 2601-2613.
80. J. M. White and G. R. Whittaker, *Traffic*, 2016, **17**, 593-614.
81. M. Lommel and S. Strahl, *Glycobiology*, 2009, **19**, 816-828.
82. R. H. Schloemer and R. R. Wagner, *Journal of virology*, 1975, **15**, 882-893.
83. G. Zhao, J. R. Perilla, E. L. Yufenyuy, X. Meng, B. Chen, J. Ning, J. Ahn, A. M. Gronenborn, K. Schulten, C. Aiken and P. Zhang, *Nature*, 2013, **497**, 643-646.
84. A. S. Reicin, A. Ohagen, L. Yin, S. Hoglund and S. P. Goff, *Journal of virology*, 1996, **70**, 8645-8652.
85. T. Dorfman, A. Bukovsky, A. Ohagen, S. Höglund and H. Göttlinger, *Journal of Virology*, 1994, **68**, 8180-8187.
86. J. A. Briggs, K. Grünewald, B. Glass, F. Förster, H.-G. Kräusslich and S. D. Fuller, *Structure*, 2006, **14**, 15-20.

TOC figure:

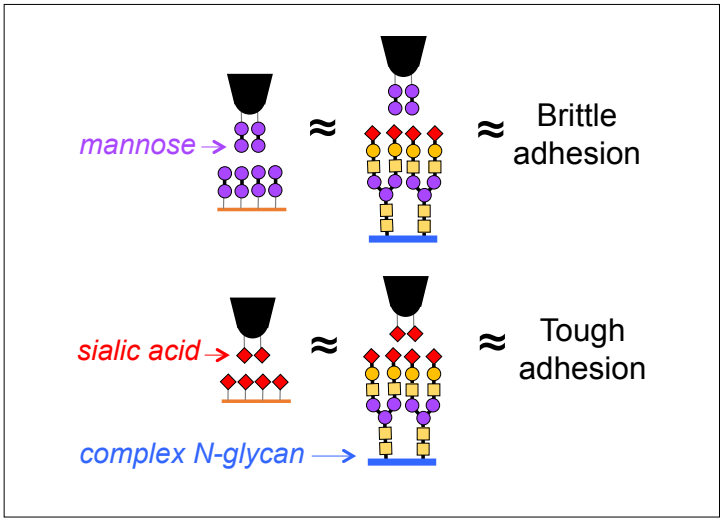

Mannose and sialic acid residues exhibit short-range brittle self-adhesion and long-range tough self-adhesion in both monolayers and complex type N-glycans.